Electronic, Optical & Structural Properties of 6.1 Angstrom III-V Semiconductor Heterostructures for High-Performance Mid-Infrared Lasers

Thomas F. Boggess

The University of Iowa
Division of Sponsored Programs
2 Gilmore Hall
Iowa City, IA 52242

December 2003

FINAL REPORT

AIR FORCE RESEARCH LABORATORY
Directed Energy Directorate
3550 Aberdeen Ave SE
AIR FORCE MATERIEL COMMAND

KIRTLAND AIR FORCE BASE, NM 87117-5776

[redacted]

DTIC COPY

This report has been approved for publication.

//signed//

ANDREW ONGSTAD, DR-II
Project Manager

//signed//

JEFFREY SALTER, MAJ, USAF
Chief, Tactical Laser Branch

//signed//

L. BRUCE SIMPSON, SES
Director, Directed Energy Directorate

REPORT DOCUMENTATION PAGE

Form Approved
OMB No. 0704-0188

1. REPORT DATE *(DD-MM-YYYY)*	2. REPORT TYPE	3. DATES COVERED *(From - To)*
December 2003	Final Report	28-Sep-01 – 26-Dec-03

4. TITLE AND SUBTITLE

Electronic, Optical & Structural Properties of 6.1 Angstrom III-V Semiconductor Heterostructures for High-Performance Mid-Infrared Lasers

5a. CONTRACT NUMBER
F29601-01-C -0229

5b. GRANT NUMBER

5c. PROGRAM ELEMENT NUMBER
61102F

6. AUTHOR(S)
Thomas F. Boggess

5d. PROJECT NUMBER
2301

5e. TASK NUMBER
LP

5f. WORK UNIT NUMBER
01

7. PERFORMING ORGANIZATION NAME(S) AND ADDRESS(ES)
The University of Iowa
Division of Sponsored Programs
2 Gilmore Hall
Iowa City, IA 52242

8. PERFORMING ORGANIZATION REPORT NUMBER

9. SPONSORING / MONITORING AGENCY NAME(S) AND ADDRESS(ES)

AFRL/DELS
3550 Aberdeen Ave SE
Kirtland AFB NM 87117-5776

10. SPONSOR/MONITOR'S ACRONYM(S)

11. SPONSOR/MONITOR'S REPORT NUMBER(S)
AFRL-DE-PS-TR-2004-1002

12. DISTRIBUTION / AVAILABILITY STATEMENT
Approved for Public Release; Distribution is Unlimited

13. SUPPLEMENTARY NOTES

14. ABSTRACT

The goal of this program was to develop new insight into the physics of 6.1-angstrom heterostructures through combined experiment and theoretical efforts. Specifically, time-resolved ultrafast optical and scanning-tunneling microscopy (STM) experimental techniques were used to study the electronic, optical, and structural properties.

15. SUBJECT TERMS 6.1 angstrom semiconductors, antimonides, mid-IR semiconductor lasers, photoluminescence upconversion, scanning-tunneling microscopy.

16. SECURITY CLASSIFICATION OF:			17. LIMITATION OF ABSTRACT	18. NUMBER OF PAGES	19a. NAME OF RESPONSIBLE PERSON
a. REPORT	b. ABSTRACT	c. THIS PAGE			Andrew Ongstad
Unclassified	Unclassified	Unclassified	Unlimited	30	19b. TELEPHONE NUMBER *(include area code)* (505) 853-3207

Standard Form 298 (Rev. 8-98)
Prescribed by ANSI Std. 239.18

TABLE OF CONTENTS

LIST OF FIGURES

INTRODUCTION

This document is the Final Report for Contract No. F29601-01-C0229, Electronic, Optical, and Structural Properties of 6.1-Angstrom III-V Semiconductor Heterostructures for High-Performance Mid-Infrared Lasers. The broad goal of this program was to develop new insight into the physics of 6.1-Å heterostructures through combined experimental and theoretical efforts. Specifically, the intent was to use time-resolved ultrafast optical and scanning tunneling microscopy (STM) experimental techniques to study the electronic, optical, and structural properties of such materials and to closely coordinate these efforts with theoretical studies based on the fundamental electronic structure of these novel materials. A particular aim has been to help to establish the knowledge base required to develop the next generation of high-power midwave infrared (MWIR) semiconductor lasers for infrared countermeasures and other Air Force applications.

The program has been multi-institutional in scope. Experimental ultrafast optical studies and all theoretical efforts were conducted at the University of Iowa (UI) under the direction of Professors Thomas Boggess (PI) and Michael Flatté (Co-PI). All STM measurements and analyses were performed at Texas A&M University (TAMU) under the direction of Professor Michael Weimer. This work was conducted in collaboration with researches at the Air Force Research Labs (Kirtland AFB) and MIT Lincoln Laboratories.

The scope of this project has been substantially reduced, relative to that originally proposed, due to a major reduction in funding ($60,000 funded compared to $300,000 proposed). This cut occurred early in the project, and the funds actually allocated provided less than one year of funding for the proposed two-year project.

This document is divided into two primary parts. We first describe ultrafast optical measurements and theoretical calculations performed at UI and then discuss the STM studies conducted at TAMU.

ULTRAFAST OPTICAL SPECTROSCOPY AND THEORY

Experiments

Carrier Recombination in IA-OPSL structures

Researchers at MIT Lincoln Laboratories and AFRL Phillips Laboratories have recently demonstrated the MBE growth of high-performance, optically-pumped, semiconductor lasers with integrated absorber regions (IA-OPSL). We have shown under prior Air Force support that transfer of carriers from the IA regions to the quantum well band edge states occurs on a time scale of tens of picoseconds and that the lifetime of carriers in the high-quality IA regions is tens of nanoseconds. This, as well as device performance, suggests an excellent efficiency for the carrier transfer process. During the current project, we performed follow up measurements of the carrier recombination in the wells themselves. Carrier dynamics in these regions are important, as electronic structure engineering of the recombination in these regions may well be an important route for further optimization.

We performed time-resolved photoluminescence (PL) upconversion measurements on three IA-OPSL samples from MIT Lincoln Laboratories: 299-057, an InAs/GaInSb/InAs multiple quantum well (MQW), 200-053, an AlGaAsSb/InAs/GaInSb/InAs/AlGaAsSb MQW, and 201-009, a GaInSb/InAs/GaInSb

MQW, all with quaternary separate absorbing barriers with band gaps near 2 μm. Example data are shown in Figure 1 for sample 201-009 at a lattice temperature of 77K. The various curves represent the PL response for varying excitation powers. All data were obtained using near-IR excitation (~ 800 nm) with ~100 fs pulses at a repetition rate of 76 MHz (roughly 13 ns between pulses). The decay of the PL is a measure of the decay of the carrier density through, in principle, all possible recombination mechanisms, e.g., Shockley-Read-Hall (SRH), interface, radiative (typically negligible in these type-II structures for the relevant carrier densities), and Auger recombination.

In principle, analysis of these data can generate a complete picture of the carrier recombination. We call attention, however, to the inset in the figure, which shows, on a semi-logarithmic scale, the PL decay for the lowest excitation level. At carrier densities corresponding to such excitation, one would expect the carrier recombination to be dominated by linear processes, such as SRH and/or interface recombination. There are two features to note in these data. First, as indicated by the solid line in the inset, the decay in all cases is somewhat nonexponential. Second, the decay is much longer than a nanosecond in sample 201-009, as it is for the other two samples. While the former result points toward what might be interesting flaw-related recombination, the latter suggests that a decreased repetition rate and an extended optical delay would be useful for these measurements.

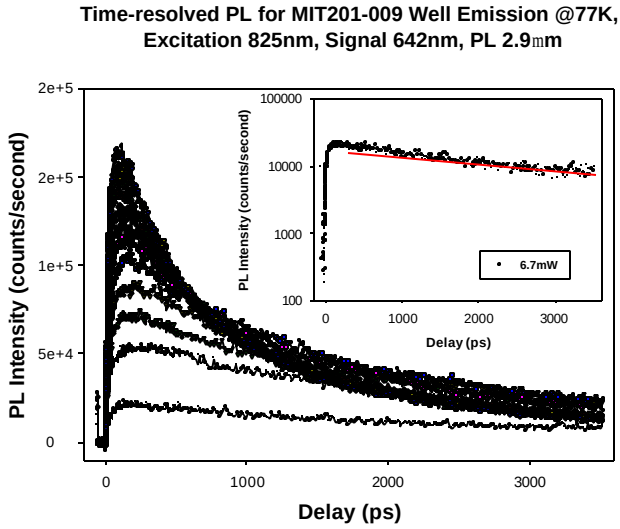

Figure 1. Time resolved photoluminescence at 77K and at varying excitation powers for sample 201-009. The inset shows a semilogarithmic plot of the lowest power data, together with an exponential fit to the data at large delays (solid line).

Based on such measurements and our interest in obtaining high-quality and quantitative measurements of the lifetimes in the IA regions, we set out to develop infrastructure that would allow us to more ably perform measurements at reduced repetition rates and over longer optical delays. Under separate funding, we acquired an electro-optic pulse picker that improved our abilities to measure carrier lifetimes in high-quality heterostructures designed for MWIR lasers. Specifically, the pulse picker allows us to reduce the repetition rate of our mode-locked Ti:Sapphire laser.

Our prior work clearly demonstrated that the quaternary IA regions in the IA-OPSLs can have lifetimes of tens of nanoseconds, but accurate determination of lifetimes this long was problematic at the time of these measurements due to the 76 MHz native

repetition rate of our mode-locked laser. Such a high repetition rate can lead to a build up of a steady-state carrier background that can result in erroneous interpretations of the density dependence of the recombination rate. For example, for a repetition period T and a recombination time τ (assuming a simple exponential decay), the carrier density at any instant of time t is:

$$N(t) = N(0)\exp(-t/\tau)/[1-\exp(-T/\tau)] ,$$

where N(0) is the carrier density generated by a single mode-locked pulse. Thus, for a typical low-density recombination time of 4 ns in an antimonide superlattice and T=13ns, the steady-state carrier background is 4% of N(0), while for a carrier lifetime of 30 ns, the steady-state background is 184% of N(0). This fractional buildup of carriers is strongly suppressed in the presence of Auger recombination, but it can nevertheless remain problematic.

The pulse picker allows us to obtain more reliable measurements of recombination in not only the quantum wells, but also in the quaternary IA materials, which can possess exceptionally long lifetimes. In addition, we constructed a “double-pass” optical delay line that allows us to scan delays over twice the range previously accessible (7ns compared to 3.5 ns in our prior configuration). The pulse picker allows us to avoid the build up of a steady-state carrier background that can result in erroneous interpretations of the density dependence of the recombination rate, and the double pass allows us to more accurately extract time constants from our data. More recently, we have constructed a 4-pass delay that provides optical delays of up to 14 ns.

We demonstrated the capabilities of the pulse picker system using an example study of a GaInAsSb epitaxial layer grown at MIT Lincoln Laboratories. Time-resolved measurements of the PL from a 3-μm-thick, p-type ($2x10^{17}$ cm^{-3}) layer of the quaternary grown lattice-matched to a GaSb were conducted as a function of repetition rate (controlled by the pulse picker).

In Figure 2 we show the normalized time-resolved PL for this sample measured at 88K using various repetition rates. For these measurements, the pulse energy was kept fixed, but the average power varied according to the repetition rate. With the pulse picker off, the rate was fixed at 76 MHz with an average power of 10 mW, while for operation at ¼ of this rate, the average power was 2.5 mW. Several features are evident in the data. First, the slow decay of the data for all repetition rates clearly indicates a long carrier lifetime in this material; fits indicate a lifetime of roughly 20 ns. Secondly, the rise in the background signal (data at negative delays) with increasing repetition rate clearly indicates a build up of a steady state carrier population at higher repetition rates, as would be expected given a 20 ns lifetime and a minimum repetition period of 13 ns. It is also evident that by reducing the repetition rate to ¼ of its maximum value, the residual background can be essentially eliminated.

Further evidence of the elimination of this steady-state population is seen in the inset, which shows the same data on an expanded time scale. The “dip” in the data near zero delay is interpreted as a transient reduction in PL associated with pump-induced heating of the residual carrier distribution. That is, the absorption of the 100 fs pump, which has significant excess energy (photon energy >> band gap energy), essentially instantaneously heats the residual distribution, thereby removing carriers from the band

edge states and reducing the PL. As the carriers cool on a picosecond time scale, the PL recovers and is enhanced by the injection of the additional carriers excited by the pump. The final feature illustrated by these data is the subtle distinction in the decay curves for the various repetition rates. These results suggest that a true measure of the carrier dynamics can be achieved only if the natural repetition rate of the laser is reduced by at least a factor of 4.

Figure 2. Time-resolved photoluminescence from a GaInAsSb sample using repetition rates of 76, 38, and 19 MHz. The inset shows an expanded view of the data near zero delay, illustrating residual carrier heating at the highest repetition.

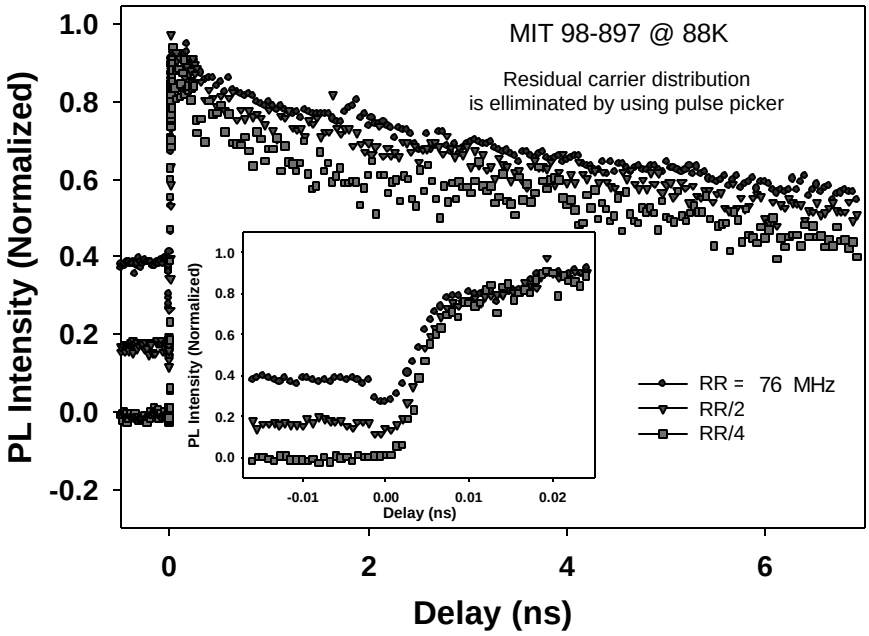

It is important to recognize that the ability to vary our repetition rate allows us to more thoroughly investigate Shockley-Read-Hall (SRH) and interface recombination in laser materials. It is possible that, even when a background PL signal is not observed, a high-repetition-rate system may result in filling of trapping levels that subsequently affect the recombination rate. It would be interesting to perform PL upconversion with the pulse picker in place to re-examine the recombination in laser structures investigated under prior support to determine whether carrier accumulation effects had any influence on our SRH results.

Theory

During this project, we completed coding and testing for including self-consistent charging effects in our band structure code. Two forms of calculation were implemented. One is most appropriate for quantum wells, and emphasizes the zone-center superlattice states. This will be most accurate when there is minimal dispersion along the growth direction in the band structure of the superlattice/quantum well. This implementation is extremely fast, and may take only a few minutes of CPU time on a desktop workstation. The other, more computationally intensive, approach is to include the full growth-direction dispersion relations in calculating the position-dependent charge density. This approach takes often a few hours to run for each iteration.

These new subroutines are intended to permit the calculation of charging effects on the band structure, including transient effects after the optical or electrical injection of carriers. As the code in general permits the calculation of photoluminescence, absorption, gain, etc., these quantities can now be calculated for transient situations and dynamically in the cooling or carrier injection process. To facilitate these and other theoretical

calculations, we acquired a 30-node Beowulf cluster. This system was purchased from another grant to assist in detailed numerical calculations, but it was made available for use on this Air Force contract. This system greatly enhanced our ability to do all of the calculations relevant to this contract.

CROSS-SECTIONAL SCANNING TUNNELING MICROSCOPY

Because of the difficulties historically attributed to the mixed-anion character of 6.1 Å semiconductor heterostructures based on GaSb and InAs, attention has understandably focused on anion segregation at the (normal) InAs-on-GaSb interface as a particularly important issue. As outlined in previous reports, we have used STM to examine the reciprocal problem of cation segregation at the (inverted) GaSb-on-InAs interface. These studies have shown that indium segregation, in fact, poses the more significant problem as intermixing within the cation sublattice frustrates attempts to maintain InSb-like bonding across the inverted heterojunction. Here we continue our analysis of the inverted heterojunction and turn attention to the question of whether or not minority segregation — that is, segregation of arsenic into antimony (the converse of what occurs at the normal heterojunction) — is also a factor comprising interfacial quality.

Our discussion again concerns two (nominal) 14-ML InAs / 28-ML GaSb multiple quantum well samples — *MQW*1 (**R0-67**) and *MQW*2 (**R0-68**) — fabricated at the University of New Mexico's Center for High Technology Materials by Dr. Ron Kaspi. Epitaxial growth was carried out with cracked arsenic and antimony sources, and combined a 12-second antimony soak at the inverted interface with a 3-second total growth interrupt at the normal interface. The schematic layer structure and interface

shutter sequencing for both samples are summarized in Figure 3. The two growths were distinguished by the maintenance of either a high (*MQW*1) or a low (*MQW*2) antimony flux, relative to fiducial conditions, during growth of GaSb as well as during an antimony soak of the inverted heterojunction. The ratio of incident-to-consumed Sb_2 (8.5:1 for *MQW*1 and 1.6:1 for *MQW*2) was determined in each case with desorption mass spectrometry (DMS). The corresponding (004) high-resolution x-ray diffraction (HRXRD) spectra are contrasted in Figure 4, which shows the two structures to have similar overlayer periodicities and relatively small mismatch with the substrate in either case. The x-ray spectra nevertheless indicate better overall structural quality in the case of *MQW*2, as evidenced both by somewhat narrower satellite peak widths and by Pendellosung fringes flanking the substrate peak.

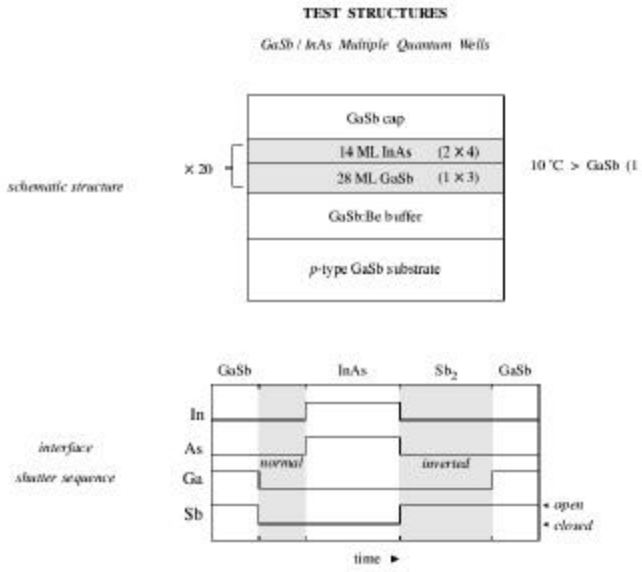

*Figure 3. The schematic layer structure and interface shutter sequencing for samples MQW1 (**R0-67**) and MQW2 (**R0-68**).*

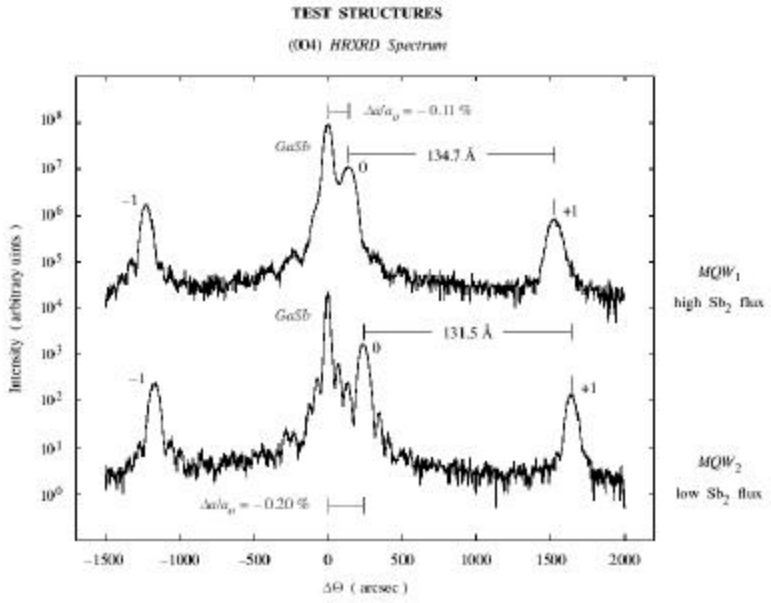

Figure 4. High-resolution X-ray diffraction for samples MQW1 and MQW2.

Figure 5 shows representative anion sublattice images from *MQW*2 illustrating the two distinct sequences of bulk layers exposed by (110) cleavage across the inverted heterojunction (carat). The upper sequence reveals the very last arsenic layer of InAs, where considerable point-like antimony (well in excess of the cross incorporated background) is evident. The lower sequence exposes the very first antimony layer of GaSb where InSb-like interface bonds are quickly recognized. Typical STM signatures for substitutional arsenic back bonded to gallium — $As_{Sb}(1)$ — from arsenic cross incorporation, substitutional antimony back bonded to indium — $Sb_{As}(1)$ — from

antimony segregation, as well as substitutional antimony back bonded to gallium from indium segregation — $In_{Ga}(2)$ — are also indicated.

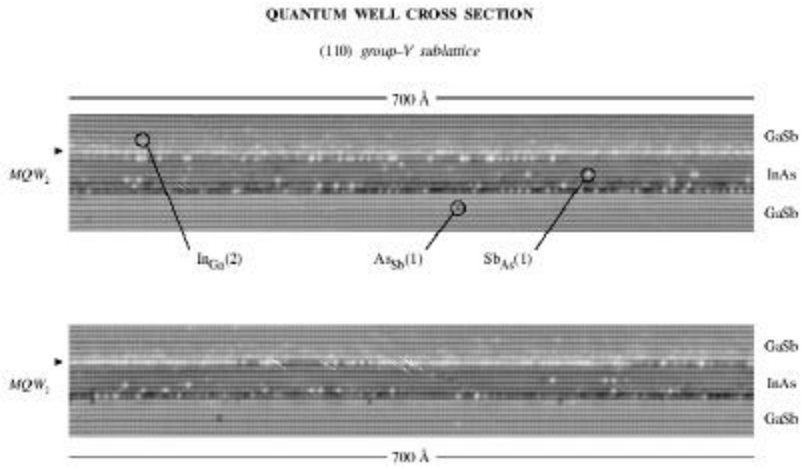

Figure 5. Representative anion sublattice images from MQW2 illustrating the two distinct sequences of bulk layers exposed by (110) cleavage across the inverted heterojunction.

Figures 6 and 7 illustrate the respective indium and arsenic impurity profiles across the inverted heterojunction, each of which were assembled from a large ensemble of STM images gathered from *MQW*1 and *MQW*2. The indium segregation profiles have previously been analyzed in detail, their most salient feature being that, in each instance, they reflect a monolayer seed that is subsequently dispersed over a dozen or so cation monolayers. The arsenic impurity profiles obtained by identifying all substitutional arsenic back bonded to gallium (within the very same image set used to assemble the indium data) are comparatively abrupt, extending no more than two anion planes into the GaSb layers.

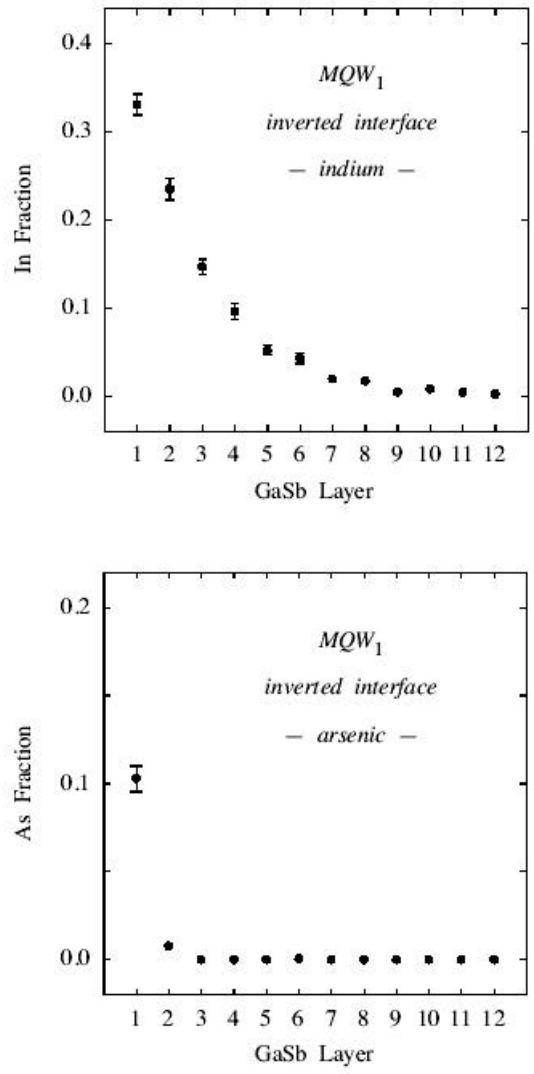

Figure 6. Indium and arsenic impurity profiles across the inverted heterojunction for MQW1.

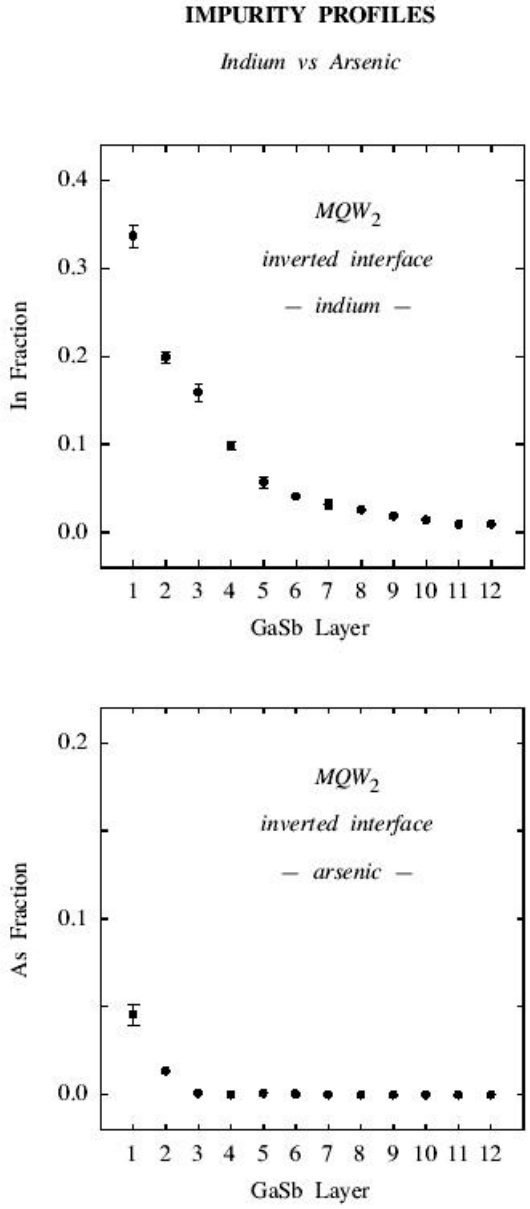

Figure 7. Indium and arsenic impurity profiles across the inverted heterojunction for MQW2.

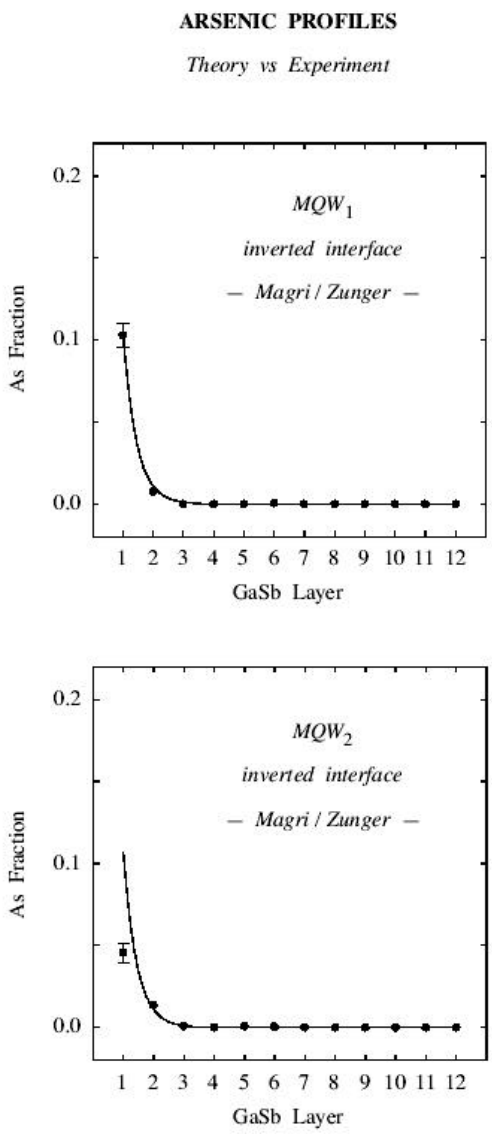

Figure 8. Comparison of experimentally determined arsenic impurity profiles with a recent calculation by Magri and Zunger [1].

Figure 8 contrasts these experimentally determined arsenic impurity profiles with a recent calculation by Magri and Zunger [1] of minority (arsenic) segregation across an

InSb-like inverted heterojunction. The calculation presumes a kinetic model of segregation (with arsenic-antimony replacement exponentially dependent on an "atomic exchange" energy $\Delta_{Sb/As} \sim 70$ meV) in the presence of a continuous vapor source of gallium and antimony. (It would appear that cation and anion segregation are simultaneously and self-consistently considered in the model but whether this is indeed so is not entirely clear.) There is surprisingly good agreement between this theory and the data for *MQW*1 but less impressive agreement in the case of *MQW*2, where the theoretical and experimental arsenic fractions in the first layer differ by more than a factor of two.

Further experimental insight is available through direct comparison of the impurity fraction and cluster distribution of substitutional arsenic in the first antimonide layer with the corresponding data for substitutional antimony within the last arsenide layer. If "atomic exchange" is indeed responsible for this substitional arsenic, one would expect a one-to-one correspondence between both the densities of, and size distributions for, the respective impurities. The requisite data are presented in Figure 9, where good agreement between arsenic (filled symbols) and antimony (open symbols) impurity fractions, as well as cluster size distributions, is found for *MQW*1 but not *MQW*2.

The disparity in the case of *MQW*2 is further emphasized by examining the probability a given impurity atom will be found within a cluster of specified size (essentially a reweighting of the cluster size distribution by the number of atoms in a given cluster). The results are presented in Figure 10, where it is immediately clear that the substitutional arsenic in *MQW*2 is essentially point like, whereas the probability distribution for substitional antimony is considerably broader. It thus appears unlikely, on account of the difference in density as well as in impurity probability versus cluster size,

that the substitutional arsenic in *MQW*2 arises from minority segregation, with antimony from the vapor settling in the anion sublattice hole that is left behind. One alternative explanation for the first-layer arsenic in *MQW*2 is incomplete antimony-for-arsenic exchange [2] during the antimony soak used to form an InSb-like interface along the inverted heterojunction (Figure 3), but this hypothesis leaves the origin of the (substantial) last-layer antimony fraction in this sample unresolved.

There are other puzzling aspects to these data as well; for example, it is somewhat surprising that theory (which presumes a perfectly flat and homogeneous InSb-like interface as its starting point) and experiment appear to be in agreement for the sample (*MQW*1) whose x-ray spectrum is of lesser quality, while for the sample (*MQW*2) of apparently superior quality, theory and experiment diverge. It is likewise mysterious why the substitutional antimony fraction within the last arsenide layer should be comparable in the two cases of high and low antimony flux whereas the substitutional arsenic fraction decreases by a factor of two with reduced antimony exposure.

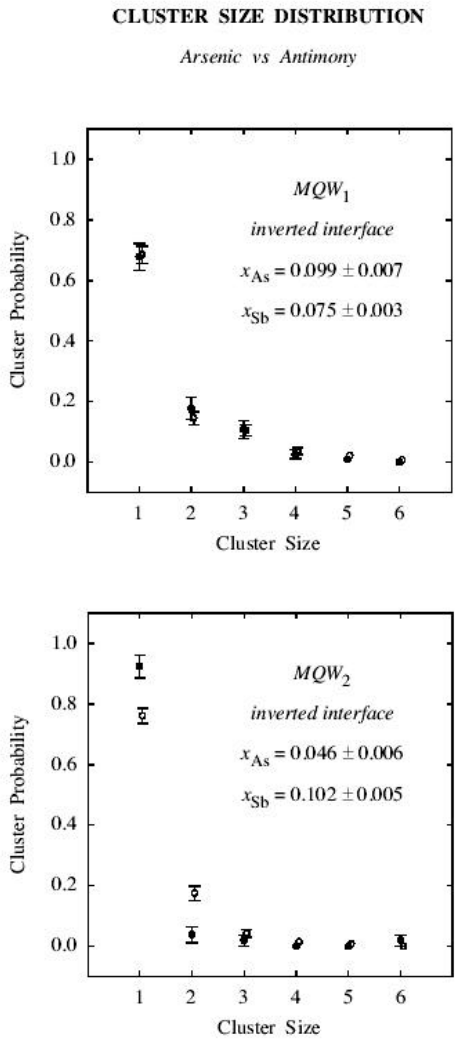

Figure 9. Comparison of cluster distribution of substitutional arsenic in the first antimonide layer with the corresponding data for substitutional antimony within the last arsenide layer. Good agreement between arsenic (filled symbols) and antimony (open symbols) impurity fractions, as well as cluster size distributions, is found for MQW1 but not MQW2.

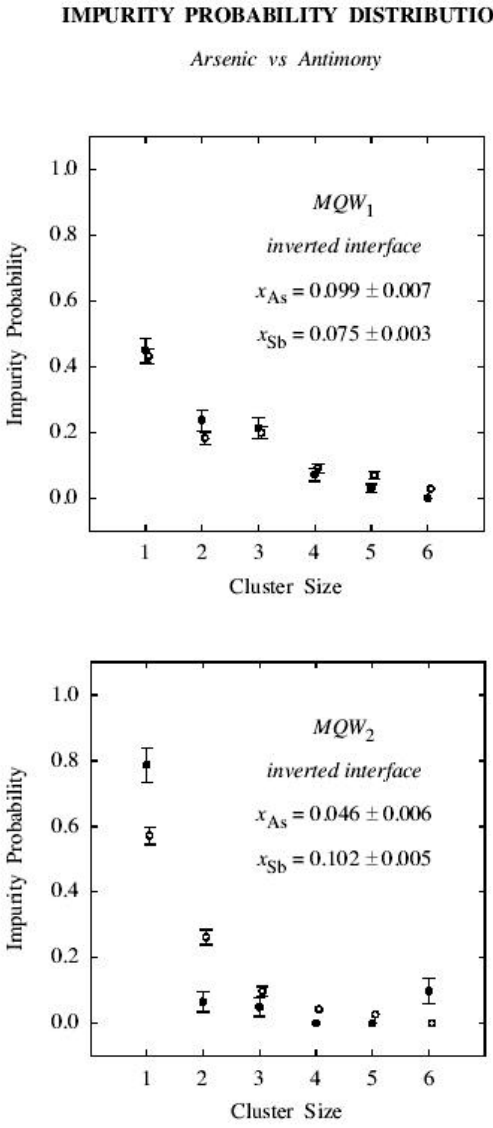

Figure 10. Probability a given impurity atom will be found within a cluster of specified size.

CONCLUSIONS

On this project, we have attempted to bring together a coherent set of techniques to advance our understanding of the 6.1- Å heterostructures relevant to MWIR lasers. Specifically, we have combined time-resolved spectroscopy, electronic structure codes, atomic-scale cross sectional STM and, through our collaborators at AFRL and MIT Lincoln Laboratory, advanced epitaxial growth to study these unique materials. In the process we have developed new tools that will help with future investigations of this material system. For example, we have developed a system for time-resolved optical measurements that not only provides a variable repetition rate, but it also allows us to produce optical delays of ~ 14 ns. This system will be useful for future studies of high quality epitaxial layers that may have SRH or interface recombination lifetimes in excess of 10 ns.

Theoretical numerical codes for electronic structure calculations have been modified to include space charge fields in a self consistent manner. These codes will be useful not only for refining calculations of the equilibrium band structure, but also for understanding the effects of internal space charge fields on nonequilibrium carrier distributions.

We continued our analysis of the inverted heterojunction and turned our attention to the question of whether or not minority segregation (i.e., segregation of arsenic into antimony) is also a factor comprising interfacial quality. The arsenic impurity profiles obtained by identifying all substitutional arsenic back bonded to gallium are comparatively abrupt, extending no more than two anion planes into the GaSb layers. Comparison of arsenic impurity profiles with the recent theory of Magri and Zunger [1] is

inconclusive, as excellent agreement is found for one quantum well (*MQW1*), but less satisfying agreement is found with a second quantum well (*MQW2*), which x-ray spectra indicate is structurally superior.

RECOMMENDATIONS

The STM data presented herein and in our prior work dramatically illustrate the structural nature of the no-common-atom interfaces of InAs/GaSb heterostructures and the difficulty associated with growing these heterostructures. It is by now well known that these interfaces strongly influence important physical properties, such as the band gap and absorption spectrum [3] and the electron spin relaxation time [4]. Moreover, recent investigations [5] of the quaternary alloy GaInAsSb heterostructures have shown that interface recombination dominates in high-quality structures. It is reasonable to assume that the low density recombination in short period InAs/GaSb superlattices, with their huge density of interfaces, may well be controlled by this process. If so, precise structuring of these interfaces would undoubtedly reduce this nonradiative process, thereby improving laser performance. All of these factors suggest that continued intensive investigations of interfaces in the 6.1- Å heterostructures should be a research priority for continued advances in long wavelength optoelectronics.

REFERENCES

[1] R. Magri and A. Zunger, *Phys. Rev.* **B64**, 081305(R) (2001) and private communication; the simulation shown in FIG. 8 is for a growth temperature of 380 °C and growth rate of 1 ML / sec.

[2] J. Harper, M. Weimer, D. Zhang, C.-H. Lin, and S.S. Pei, *Appl. Phys. Lett.* **73**, 2805 (1998).

[3] R. Kaspi, C. Moeller, A. Ongstad, M.L. Tilton, D. Gianardi, G. Dente, P. Gopaladasu, Appl. Phys. Lett. **76**, 409 (2000); W.H. Lau, M.E. Flatte, Appl. Phys. Lett. **80**, 1683 (2002).

[4] J.T. Olesberg, W.H. Lau, M.E. Flatte', C. Yu, E. Altunkaya, E.M. Shaw, T.C. Hasenberg, T.F. Boggess, Phys. Rev. B, **64**, 201301 (2001).

[5] D. Donetsky, S. Anikeev, G. Belenky, S. Luryi, C.A.Wang, G. Nichols, Appl. Phys. Lett. **81**, 4769 (2002).

DISTRIBUTION LIST

DTIC/OCP 8725 John J. Kingman Rd, Suite 0944 Ft Belvoir, VA 22060-6218	1 cy
AFRL/VSIL Kirtland AFB, NM 87117-5776	1 cy
AFRL/VSIH Kirtland AFB, NM 87117-5776	1 cy
Official Record Copy AFRL/DELS/Andrew Ongstad	2 cys